Mass Spectrometric Studies of Oxides

N. S. Jacobson

Structures and Materials Division, NASA Glenn Research Center,
Cleveland, OH 44135 USA

Current studies at NASA Glenn on oxide thermodynamics are discussed. Previous studies on the vaporization of B_2O_3 in reducing atmospheres led to inconsistent studies when B was used as a reductant. It is shown that liquid B_2O_3 does not wet B and a clear phase separation was noted in the Knudsen cell. This problem was solved by using FeB and Fe_2B to supply a different and constant activity of B. The thermodynamic data thus derived are compared to quantum chemical composite calculations. A major problem in high temperature mass spectrometry is the determination of accurate ionization cross sections, particularly for molecules. The method of Deutsch and Mark shows promise and some sample calculations are discussed. Finally current studies on the thermodynamics of rare earth silicates are discussed. Here the problems are obtaining a measurable signal from SiO_2 vaporization and non-equilibrium vaporization. The use of a Ta reducing agent provides a stronger signal, which is related to silica activity. The Whitman-Motzfeld relation adapted to KEMS measurements is applied to obtain equilibrium pressures.

Introduction

Oxides are used in numerous high temperature applications. It is essential to accurately measure their vaporization and thermodynamic properties and Knudsen Effusion Mass Spectrometry (KEMS) is particularly suitable for this. However, there are numerous special considerations when applying this technique to oxide systems (1). In this paper we discuss recent work at the NASA Glenn Research Center related to oxide systems. These are the vaporization of B_2O_3 in reducing environments (2), the calculation of ionization cross sections using the Deutsch-Mark method (3), and measurements of the thermodynamic activity of silica in the Y_2O_3-SiO_2 system.

Experimental

The KEMS used for these studies has been described in more detail elsewhere (4) and will only be briefly summarized here. The basic instrument is a Nuclide/MAAS/Patco 12-90-HT (12" radius, 90°) single focusing magnetic sector instrument, which has been extensively modified.

Two Knudsen cell configurations are used with this instrument—a single cell flange shown in Fig. 1 and a multiple cell flange shown in Fig. 2. The single cell flange uses a Ta 'hairpin' type resistance furnace and is capable of temperature in excess of 2000K. The multiple cell flange uses a sheet element of Ta and is capable of temperatures to about 2000K. More details on the multiple cell flange are found in another paper in this proceedings volume (5).

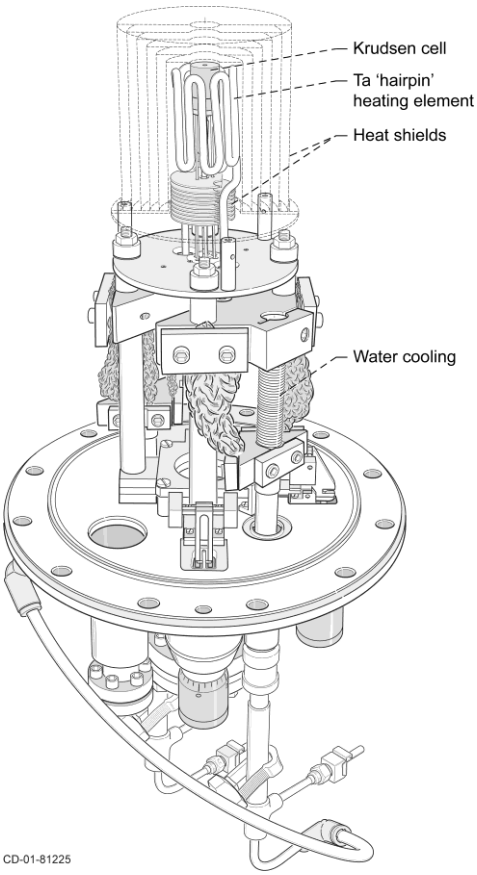

Figure 1. Diagram of the single cell/ furnace flange.

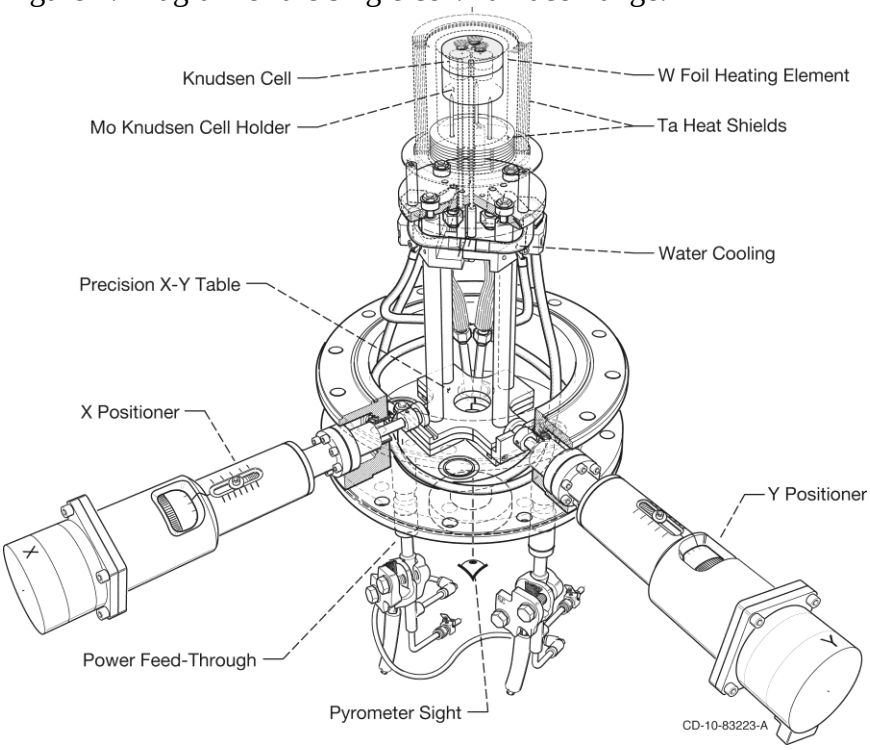

Figure 2. Diagram of multiple cell/furnace flange.

The ionization chamber in the NASA Glenn instrument is a cross-axis type, with the molecular, electron, and ion beams all mutually perpendicular. The instrument has been modified for "restricted collimation" (4-6) which gave improved reproducibility of signals and minimized spurious signals for both the single and multiple cell vapor sources.

Detection is conducted entirely with ion counting. The use of ion counting, magnetic sorting, and a non-magnetic ion source discards in principle any mass discrimination effects. Data are collected with automated multiple peak scans (5).

Vaporization of B_2O_3 in Reducing Environments

The vaporization of B_2O_3 is important in a variety of high temperature applications, including the addition of a B sintering aid to SiC ceramics and oxidation of high temperature borides. B_2O_3 vaporizes to B_2O_3(g) and B_2O_2(g). An examination of previous literature indicates that there is good agreement on the thermodynamic data for B_2O_3(g); however, there is some disagreement on the thermodynamic data for B_2O_2(g) when B is used as a reducing agent (2). In this study, we re-examine the reaction of B_2O_3(l) and B to understand this problem and generate more reliable data for B_2O_2(g). In addition quantum chemical composite methods were used to calculate thermodynamic data for B_2O_2(g).

Experimentally, our single Knudsen cell vapor source was used for these studies with a BN Knudsen cell. Temperatures were measured with a disappearing filament optical pyrometer. Initial experiments were conducted with B and B_2O_3 powders. The measured ion intensities of $B_2O_2^+$ were not reproducible and decreased throughout the experiment, as shown in Fig. 3. An examination of the cell after the experiment showed a clear phase separation between B and B_2O_3(l), as shown in Fig. 4(a).

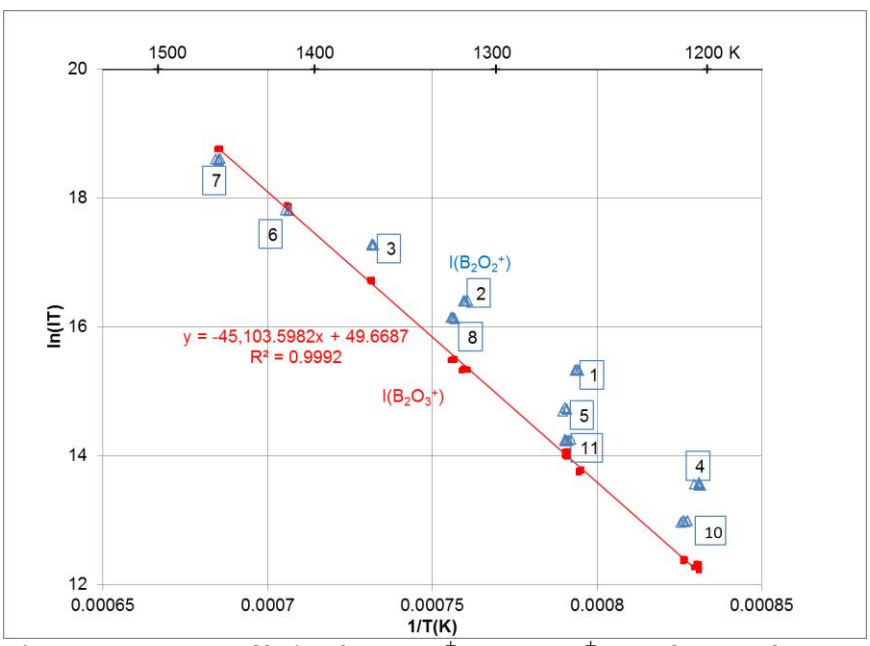

Figure 3. Van't Hoff plot for $B_2O_2^+$ and $B_2O_3^+$ ions formed from B_2O_3 and B interactions. Numbers indicate the order of taking data.

The observed phase separation clearly led to a decrease in contact area between the two condensed phases. In order to more tightly control the conditions within the cell, the B activity was fixed (albeit at a value less than unity) by adding a mixture of FeB and Fe_2B to B_2O_3. We observed In this case that the mixture remains intimately mixed after an experiment, as shown in Fig. 4(b) and probably the evaporation conditions remains the same within our temperature range for measurements. Now the Van't Hoff plot was linear with reproducible data points and it was possible to extract accurate heats of vaporization, as shown in Fig. 5

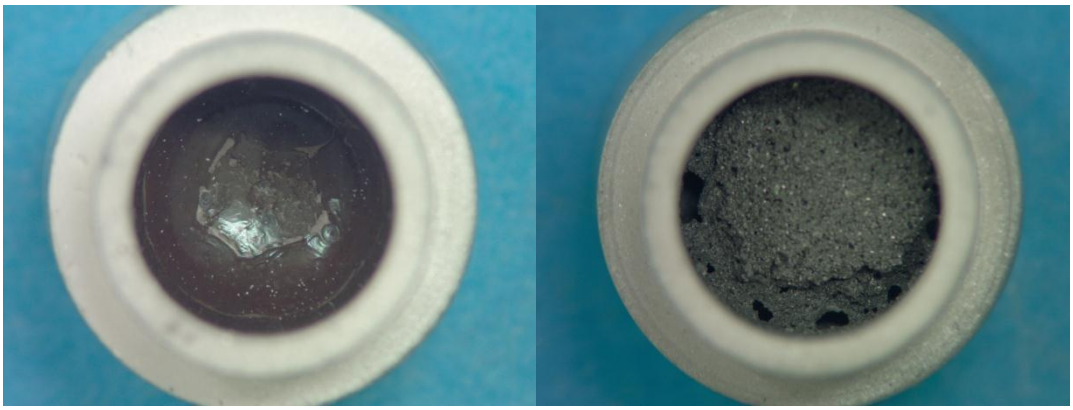

(a) (b)

Figure 4. View of cell bottom after an experiment. (a) B + B_2O_3(l) showing the phase separation (b) FeB + Fe_2B + B_2O_3(l) showing the compounds remain intimately mixed (reprinted with permission from (2)).

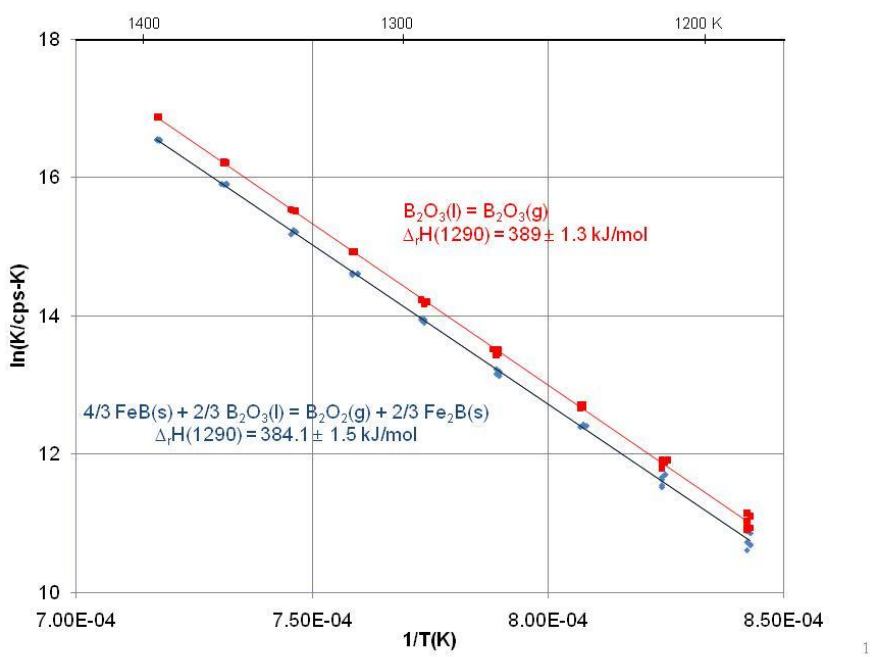

Figure 5. Van't Hoff plot for $B_2O_2^+$ and $B_2O_3^+$ ions formed from a mixture of B_2O_3, FeB, and Fe_2B (reprinted with permission from (2)).

From these data, it was now possible to extract enthalpies of formation of $B_2O_3(g)$ and $B_2O_2(g)$ at 298K. The 'sigma-plot' method was used with the second law data to extract the enthalpy of formation at 298K (7). The standard third law method was also used (8). These data are given in Tables I(a) and (b) for $B_2O_3(g)$ and $B_2O_2(g)$, respectively and compared to literature data.

Enthalpies of formation were also calculated via quantum chemical composite methods and listed in Table I(a) and (b) (9, 10). Equilibrium geometry was calculated at the B3LYP/VTZ+1 level. The W1BD method was used with a aug-cc-VnZ (n = D, T, or Q) basis set. Calculations included relativistic corrections and spin-orbit coupling effects. The W1BD method is essentially a modification of the W1 method with Brueckner Doubles to simplify the calculation (11). Calculations were done with both GAMESS (12) and Gaussian software (13). Enthalpies of reaction were determined from the reactions indicated in Tables I(a) and (b) where all other reactants and products have known enthalpies of formation. In general isogyric (constant spin) reactions are preferred.

TABLE I(a). Enthalpies of formation (kJ/mol) at 298.15K for $B_2O_3(g)$.

Selected Studies Investigator/method and reactions	**$\Delta_f H(298)$ Second Law**	**$\Delta_f H(298)$ Third Law**	**$\Delta_f H(298)$ ab initio**
Hildenbrand et al (Torsion) (14) $B_2O_3(l) = B_2O_3(g)$	-825.9	-836	
Scheer (Torsion) (15) $B_2O_3(l) = B_2O_3(g)$	-848.2	-829.2	
Shultz et al. (KEMS/Weight loss) (16) $B_2O_3(l) = B_2O_3(g)$	-841.3 ± 8.8	-837.9 ± 2.5	
Nguyen et al. (17) ab initio $B_2O_3(g) = 3B(g, doublet) + 2O(g, triplet)$			-830.1
Jacobson and Myers This study (KEMS) (2) $B_2O_3(l) = B_2O_3(g)$	-843.3 ± 6.6	-823.6 ± 1.0	
Jacobson and Myers This study (ab initio) (2) $B_2O_3(g) = 3B(g, doublet) + 2O(g, triplet)$			-857.4 ± 17.2
Jacobson and Myers This study (ab initio) (2) $B_2O_3(g) + 6HF(g) = 2BF_3(g) + 2H_2O(g)$			-831.8 ± 5.3

TABLE I(b). Enthalpies of formation (kJ/mol) at 298.15K for $B_2O_2(g)$.

Selected Studies Investigator/method and reactions	**$\Delta_f H(298)$ Second Law**	**$\Delta_f H(298)$ Third Law**	**$\Delta_f H(298)$ ab initio**
Inghram (KEMS) (18) 2/3 B + 2/3 $B_2O_3(l)$ = $B_2O_2(g)$	-509.4	-444.1	
Inghram (KEMS) (18) 2/3 B + 2/3 $B_2O_3(g)$ = $B_2O_2(g)$	-455.2	-458.7	
Scheer (Torsion) (19) 2/3 B + 2/3 $B_2O_3(l)$ = $B_2O_2(g)$	-428.6	-462.9	
Rentzepis et al. (Collection) (20) C(s) + $B_2O_3(l)$ = $B_2O_2(g)$ + CO(g)		-466.2	
Searcy and Myers (21) 2MgO(s) + 2B(s) = 2Mg(g) + $B_2O_2(g)$		-458.9	
Nguyen et al. (17) ab initio $B_2O_2(g)$ = 2B(g, doublet) + 2O(g, triplet)			457.7
Jacobson and Myers This study (KEMS) (2) 4/3 FeB(s) + 2/3 $B_2O_3(l)$ = $B_2O_2(g)$ + 2/3 $Fe_2B(s)$	-484.8 ± 25.7	-474.6 ± 25.7	
Jacobson and Myers This study (ab initio) (2) $B_2O_2(g)$ = 2B(g, doublet) + 2O(g, triplet)			-479.9 ± 17.2
Jacobson and Myers This study (ab initio) (2) $B_2O_2(g)$ + 6HF(g) = $2BF_3(g)$ + $2H_2O(g)$ + $H_2(g)$			-456.7 ± 5.3

In summary, this study explains the problems with the B + $B_2O_3(l)$ reaction. The use of FeB/Fe_2B removes this problem, but unfortunately the uncertainty in the thermodynamic data for FeB and Fe_2B (2) gives a larger error band on the heat of formation for $B_2O_2(g)$.

The values calculated from ab initio methods show reasonable agreement to the experimental values. *This study shows that coupling quantum chemical composite methods with experimental methods gives improves confidence in both approaches. Such an approach is valuable for the study of other compounds with the goal of obtaining consistent and reliable thermodynamic quantities.*

Ionization Cross Sections

The primary relationship in KEMS is the relationship of vapor pressure of species *i*, P_i, to ion intensity, I_i:

$$P_i = kI_iT/\sigma_i \qquad [1]$$

Note that this is an ideal form, where the species, *i*, forms an ion with no fragmentation. Here *k* is the instrument constant and σ_i is the ionization cross section of the species *i*.

There have been numerous experimental and theoretical studies of ionization cross sections. These are summarized in the recent review by Drowart et al. (22). First consider atomic cross sections. Generally the most commonly used calculations are those of Mann (23), who calculates cross sections by summing over radii of the outer orbitals. These have been put into a code by Bonnell and Hastie (24), which conveniently scales the calculated sections with energy of the ionizing electrons. Cross sections for molecules are more complex. It is generally agreed that some type of summation over the constituent atoms is the correct approach (25). Many investigators sum the atomic cross sections and multiply by a correction factor of 0.75 (1, 26**).**

Recently, Deutsch and Mark have developed a semi-empirical method for calculating atomic and molecular cross sections (3). This method is based on summation of orbital radii and scales to energy of the ionizing electrons. A Mulliken population analysis (27) is used for extension to molecules. This method seems particularly well-suited for cross section calculation in KEMS (28).

The basic relation for the Deutsch-Mark (D-M) method is:

$$\sigma = \sum_{n,l} \pi\, r_{n,l}^2\, g_{n,l}\, N_{n,l}\, f(u)$$

$$f(u) = \frac{1}{u}\left(\frac{(u-1)}{(u+1)}\right)^a \left[b + c\left(1 - \frac{1}{2u}\right)\ln\left(2.7 + (u-1)^{1/2}\right)\right] \qquad [2]$$

$$u = \frac{E}{E_{n,l}}$$

Here σ is the cross section, $r_{n,l}$ is the orbital radii; $g_{n,l}$ is a weighting factor; $N_{n,l}$ is the number of electrons in the particular orbital; *f(u)* is a scaling factor to give the proper dependence on electron energy; a, b, and c are parameters for the particular orbital; *E* is energy of the ionizing electrons, and $E_{n,l}$ is the energy of the particular oribital. The quantities of $r_{n,l}$ and $E_{n,l}$ are taken from the calculations of Desclaux (29). A simple spreadsheet program has been developed at NASA Glenn for determining cross sections as a function of electron energy for the elements H through Rn (30) and is available from the author.

The extension to molecules involves calculation of a Mulliken population distribution, which is easily done from various computational chemistry codes (12, 13). The Mulliken distribution is substituted for $N_{n,l}$ in the above equation and the total cross section is obtained from summing over each atom. An example of the cross section calculated via the Deutsch-Mark method and the summation of the Mann atomic sections with the 0.75 correction factor is illustrated in Fig. 6. Clearly comparison need to be made to measured cross sections to determine the best method for KEMS.

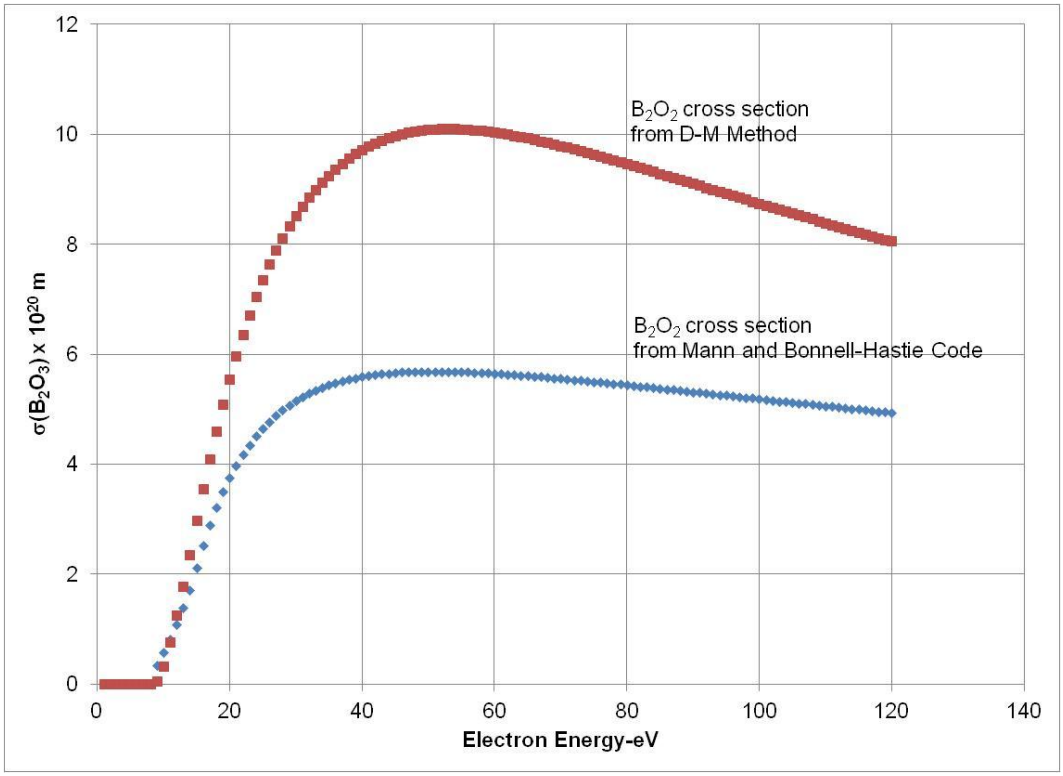

Figure 6. Calculated cross sections for $B_2O_2(g)$ via the Deutsch-Mark method and Mann and Bonnell-Hastie code.

Measurement of Thermodynamic Activities in Rare Earth Silicates

There has been a continuing interest in replacing superalloys with ceramics in heat engines and combustion applications. Research at NASA Glenn has shown that silicon-based ceramics are quite susceptible to react with the water vapor component in a combustion application (31, 32). At high temperatures, the surface oxidizes continuously meanwhile the oxidation product is volatilizing:

$$SiC(s) + 3/2\ O_2(g) = SiO_2(s) + CO(g) \qquad [3a]$$

$$SiO_2(s) + 2H_2O(g) = Si(OH)_4(g) \qquad [3b]$$

This leads to a net recession of the material surface.

In order to limit this oxidation/volatilization phenomenon, refractory oxide coatings have been proposed (33). Many of the candidate coatings have a silica component and it is essential that the thermodynamic activity of silica be as low as possible. Rare earth silicates have many desirable properties as candidate coatings (adherence, thermal expansion matching, etc.). These oxides may be treated as pseudo-binary compounds and solutions with the components Y_2O_3 and SiO_2. The phase diagram indicates a monosilicate and a disilicate compound. Thermodynamics predicts that the compounds on the Y_2O_3-rich side of the phase diagram have the lower silica

activities. For quantitative modeling it is essential to accurately know the activity of silica in these materials.

There are numerous measurements of silica activity in silicates using KEMS in the literature (1). Such measurements are complex due to several issues (1) A vapor specie which clearly varies with silica activity must be identified (2) high temperatures are required to obtain a measurable vapor pressure above SiO_2 and (3) Non-equilibrium vaporization is often a problem and must be accounted for.

Silica is well known to vaporize primarily as follows:

$$SiO_2(s) = SiO(g) + \tfrac{1}{2} O_2(g) \qquad [4]$$
$$SiO_2(s) = SiO(g) + O(g)$$

Thus the activity of silica in a silicate is defined as:

$$a(SiO_2) = \frac{p(SiO)^{soln}\left[p(O_2)^{soln}\right]^{1/2}}{p(SiO)^{o}\left[p(O_2)^{o}\right]^{1/2}} \qquad [5]$$

Here *p* is the measured pressure and the superscripts 'soln' and 'o' indicate the solution and pure SiO_2 compound, respectively. Unfortunately, in the case of rare earth silicates over the temperature range of interest (1400-1700K), this method cannot be applied, because the vapor pressure of SiO generated by reaction [4] is not measurable in the mass spectrometer.

We used Ta to impose reducing conditions to the silicates that generate a measureable signal of SiO(g) at the lower temperatures. This is similar to the approach of Zaitsev and Mogutnov (34). They use a reductant to generate measureable vapor pressures from both components in a particular silicate and then use a ratio method. In our case the reductant only generates a measurable vapor pressure for the silica component and this is measured directly with our multiple cell system. Ta reacts with SiO_2 as follows:

$$4Ta(s) + 4\underline{SiO_2}(soln) = 3SiO(g) + Ta_2O_5\,(s) + Ta_2Si\,(s) \qquad [6a]$$

$$2Ta(s) + 2\underline{SiO_2}(soln) = 2SiO(g) + TaO(g) + TaO_2(g) \qquad [6b]$$

Here the underline of SiO_2 indicates it is of less than unit activity. Equation [6a] applies to activities of silica equal from unity to about 0.02, depending on temperature. We have mixed SiO_2 powder with excess Ta and heated to 1700K and nearly all the silica reacts to form Ta_2O_5 (s) and Ta_2Si (s) as revealed by XRD. Equation [6b] applies to activities of silica less than about 0.02. A mixture of Ta + Y_2O_3 + $Y_2O_3{\cdot}(SiO_2)$ contained only these phases after heating to 1700K, as revealed by XRD. Reaction [6b] is the key reaction for the range of $a(SiO_2)$ we are interested in. Fig. 7 presents the calculated SiO(g) pressures using the FactSage (35) free energy minimizer computational thermochemistry code. Different P(SiO) correspond to different activities of SiO_2. The Ta/TaO/TaO_2 in equation (6b) fix a constant $P(O_2)$ and P(O), regardless of SiO_2 activity.

For these experiments, the multiple Knudsen cell flange was used (Fig. 2(b)) with an Au standard. In all experiments, the triple point of Au was measured to extract a temperature calibration and the machine constant (k factor in relation [1]). In addition a second law heat of Au was always measured concurrently with the measurements of SiO ion intensities. A second law heat within several kJ of the accepted value (1-2%) indicated the instrument was working properly. Representative data are shown in Fig. 8.

As discussed, another important consideration with silicates is non-equilibrium vaporization (36). The usual method of obtaining an equilibrium vapor pressure under such conditions is to apply the Whitman-Motzfeld equation (37):

$$P_m\left[1+f\left(\frac{1}{\alpha_c}+\frac{1}{W_A}-2\right)\right]=P_{eq}$$

$$f=W_B B/A \qquad [7]$$

Here P_m is the measured vapor pressure, f is given by the expression above, α_c is the condensation coefficient (assumed equal to the vaporization coefficient in this analysis), W_A is the Clausing factor for the cell, P_{eq} is the equilibrium vapor pressure, W_B is the Clausing factor for the orifice, B is the cross sectional area of the orifice, and A is the cross sectional area of the cell. Generally measurements are taken with a series of orifice sizes and a plot of Pm vs Pmf extrapolates to the equilibrium vapor pressure and the slope of the resultant line is related to the condensation coefficient.

Chatillon and co-workers have extended the Whitman-Motzfeld analysis to a multi-cell KEMS method. For our cells, we used the following equations to derive a condensation coefficient:

$$\frac{1-\left(\frac{I_i}{I_j}\right)}{f_j-f_i\left(\frac{I_i}{I_j}\right)}=-\left(\frac{1}{k\alpha}-0.51\right) \qquad (8)$$

In this case several pairs of cells are used with different orifice sizes, f factors, and hence intensities, designated by I_i, f_i and I_j, f_j, respectively. Here k is a geometry factor between 0 and 1, which accounts for the lack of an atomically flat surface. A plot of measured condensation coefficients is shown in Fig. 9. These were used to obtain an equilibrium ion intensity from the Whitman-Motzfeld equations above. The equilibrium ion intensity was in turn converted to the equilibrium P(SiO).

The equilibrium ion intensity was in turn converted to an equilibrium P(SiO) using the calibrated constant derived from the triple point of Au and the appropriate cross sections (3). From this P(SiO) and plot similar to Fig. 7 for each temperature, the activity of SiO_2 was determined for the Y_2O_3 + $Y_2O_3{\cdot}(SiO_2)$ phase field. The results are given in Fig. 10. These are compared to the optimization of Fabrichnaya and Seifert (38) obtained from mainly phase diagram data (due to the lack of thermodynamic data at the time of the optimization).

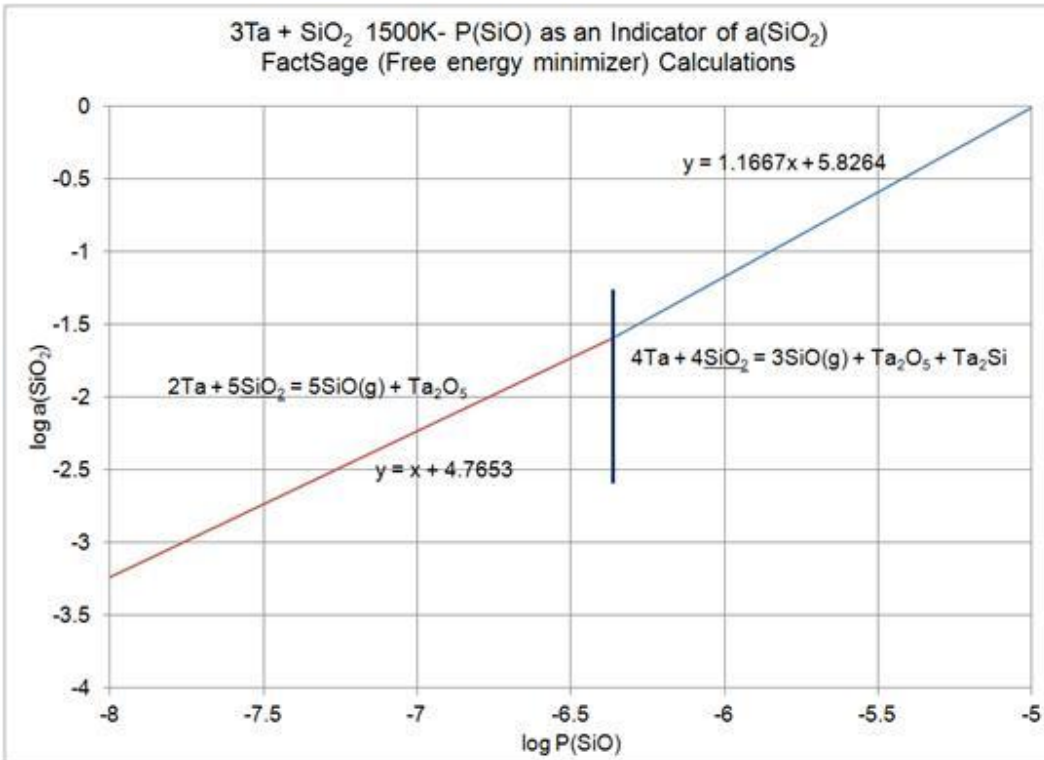

Figure 7. Vapor pressure of SiO(g) obtained by thermodynamic calculations for mixtures of SiO_2 and excess Ta.

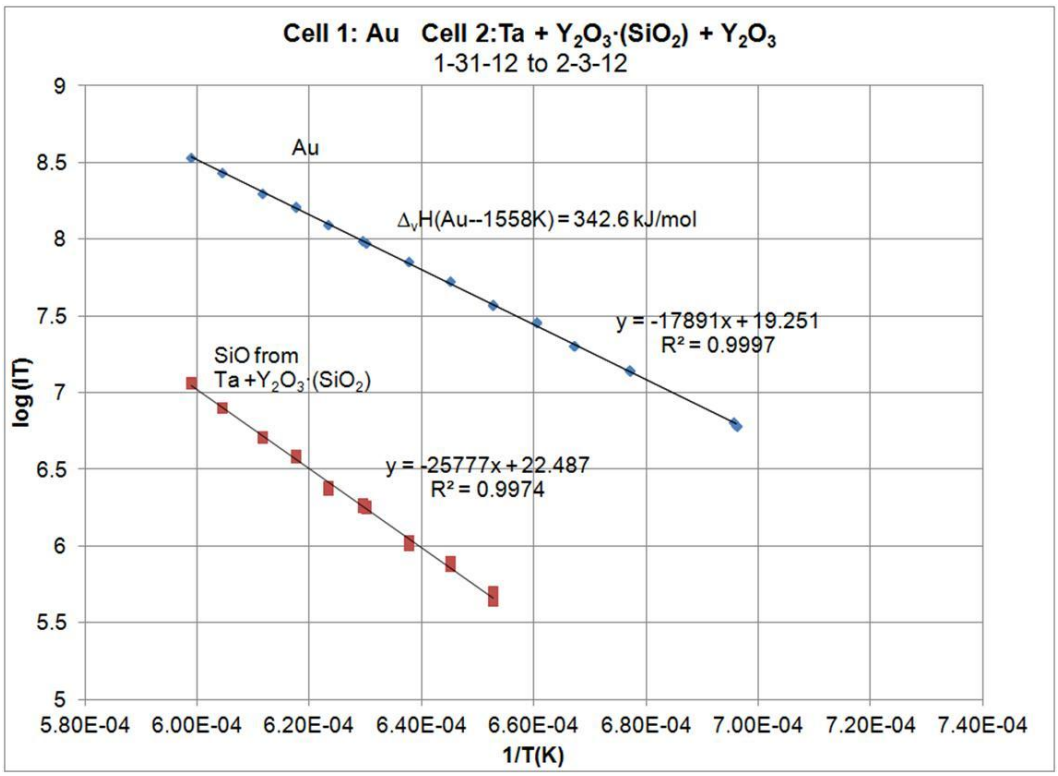

Figure 8. The product of ion intensity with temperatures as a function of inverse temperatures for Au in cell 1 and Ta + Y_2O_3 + $Y_2O_3{\cdot}(SiO_2)$ mixture in cell 2.

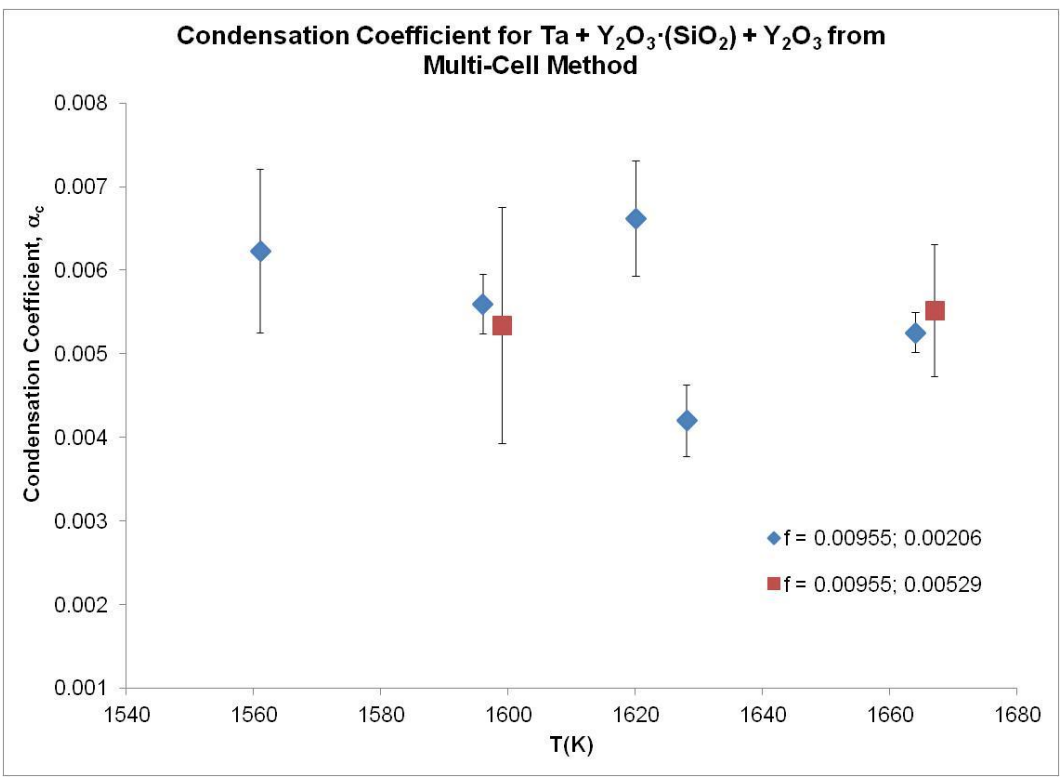

Figure 9. Determined condensation coefficients for the SiO(g) molecule using ionic intensity comparison between two different cells (characterized by their f factors) in the multiple cell method.

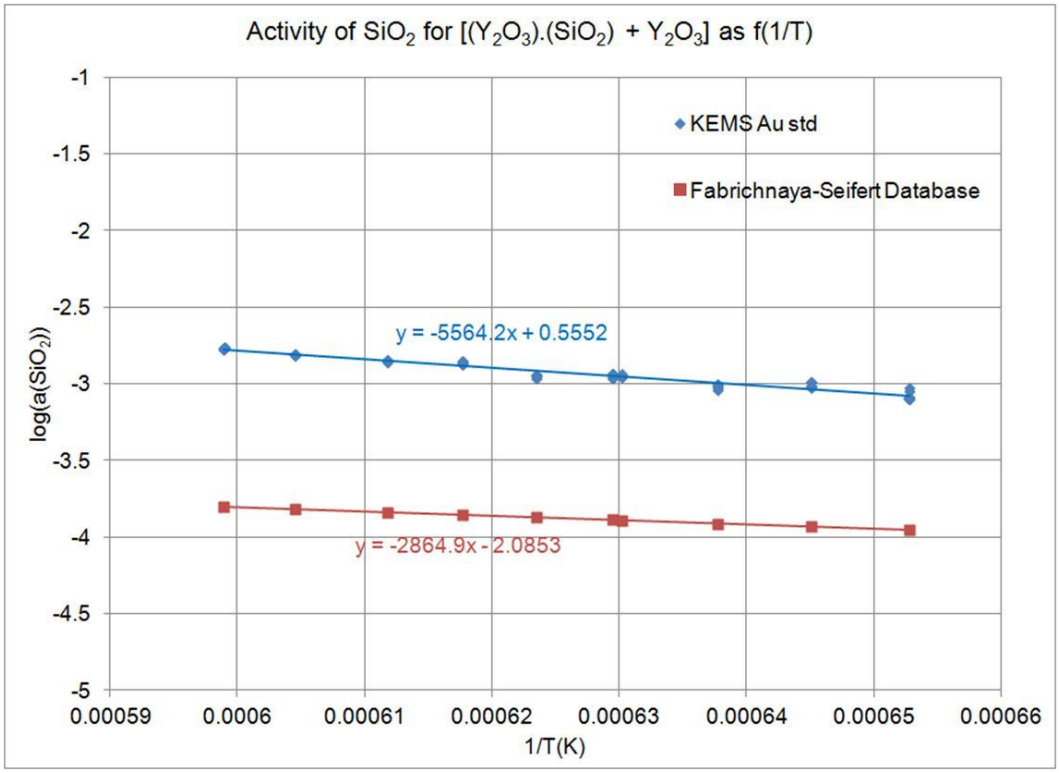

Figure 10. Measured activity in the $Y_2O_3{\cdot}(SiO_2)$ + Y_2O_3 phase field, compared to the optimization performed of Fabrichnaya and Seifert (38).

Conclusions

Recent work at NASA Glenn on KEMS of oxides has been discussed. A study on the vaporization of B_2O_3 in reducing atmospheres has been summarized. In this study the problem of maintaining contact area between B_2O_3(l) and the reducing agent was addressed by using FeB + Fe_2B to set a boron activity instead of pure B. Experimental measurements were compared with quantum chemistry composite calculations. Such an approach provides a check for the consistency of both methods and is thus quite valuable. In oxide studies by KEMS, ionization cross sections are particularly important. The Deutsch-Mark semi-empirical method of calculating cross sections for atoms and molecules was discussed in regard to KEMS applications in order to improve the accuracy of partial pressure determinations. Finally recent work on measurement of thermodynamic activities of silica in rare earth silicates was discussed. Ta is used as a reducing agent in order to provide a stronger SiO(g) signal, which remains related to silica activity. Non-equilibrium vaporization is also accounted for. The present thermodynamic results for the $Y_2O_3{\cdot}(SiO_2)$ + Y_2O_3 pseudo-binary phase field and indicate that additional thermodynamic data are necessary to improve the existing optimization.

Acknowledgments

It is a pleasure to thank Dr. Evan Copland (now with CSIRO, Sydney, Australia), who worked at NASA Glenn for 10 years and modified the NASA instrument for restricted collimation and constructed the multi-cell flange. These two changes improved the performance dramatically. Thanks are also due to Prof. Dwight Myers of East Central University, Ada, OK, who performed the quantum chemistry composite calculations for both the boron oxide thermodynamics and cross section calculations.

References

1. V. L. Stolyarova, G.A. Semenov, and J.H. Beynon, *Mass Spectrometric Study of the Vaporization of Oxide Systems*, Wiley, Chichester (1994).
2. N. S. Jacobson and D.L. Myers, *J. Phys. Chem. B*,. **115**(45), 13253-13260 (2011)..
3. H. Deutsch, et al., in. *Advances in Atomic, Molecular, and Optical Physics*, **57**,. 87-155 (2009).
4. E. H. Copland and N.S. Jacobson, *Measuring Thermodynamic Properties of Metals and Alloys with Knudsen Effusion Mass Spectrometry*, NASA/TP—2010-216795.
5. E. H. Copland, J. V. Auping, and N. S. Jacobson. in *Workshop on Knudsen Effusion Mass Spectrometry*. T. Markus and N. Jacobson, Editors, The Electrochemical Society Proceedings Series (2012).
6. P. Morland, C. Chatillon, and P. Rocabois, *H. Temp. and Mat. Sci.*, **37**(3), 167-187 (1997).
7. D. Cubicciotti, *J. Phys. Chem.*, **70**(7), 2410-2413 (1966).
8. J. Drowart and P. Goldfinger, *Angew. Chem.-Intl. Ed*, **6**(7), 581-648 (1967).
9. J. M. L. Martin and G. de Oliveira, *J. Chem. Phys.*, **111**(5), 1843-1856 (1999).
10. S. Parthiban and J.M.L. Martin, *J. Chem. Phys.*, **114**(14), 6014-6029 (2001).
11. R. Kobayashi, et al., *J. Chem. Phys.*, **95**(9), 6723-6733 (1991).
12. M. S. Gordon and M.W. Schmidt, in *Theory and Applications of Computational Chemistry, the First Forty Years*, C.E. Dykstra, et al., Editors, Elsevier, Amsterdam (2005).
13. Frisch, M.J., et al., *Gaussian 09, Revision B.01*, Gaussian, Inc., Wallingford, CT (2010).
14. D. L. Hildenbrand, W.F. Hall, and N.D. Potter, *J. Chem. Phys.*, **39**(2), 296-301 (1963).
15. M. D. Scheer, *J. Phys. Chem.*, **61**(9), 1184-1188 (1957).
16. M. M. Shultz, V. L. Stolyarova, and G. A. Semenov, *Fizika i Khimiia Stekla*, **4**(6), 653-661 (1978).
17. Nguyen, M.T., et al., *J. Phys. Chem. A*, **113**(17), 4895-4909 (2009).
18. M. G. Inghram, R. F. Porter, and W. A. Chupka, *J. Chem. Phys.*, **25**(3), 498-501 (1956).
19. M. D. Scheer, J. Phys. Chem., **62**(4), 490-493 (1958).
20. P. Rentzepis, D. White, and P. N. Walsh,. J. Phys. Chem., **64**(11), 1784-1787 (1960).
21. A. W. Searcy and C. E. Myers, *J. Phys. Chem.*, **61**(7), 957-960 (1957).
22. Drowart, J., et al.,. *Pure Appl. Chem.*, **77**(4), 683-737 (2005)..
23. Mann, J.B., J. Chem. Phys., **46**(5), 1646-1651 (1967).

24. Bonnell, D.W., *Sigma Fortran Program*, National Institute of Standards and Technology, (1990).
25. J. W. Otvos and D.P. Stevenson, J. Am. Chem. Soc. **78**(3), 546-551 (1956).
26. K. Hilpert, *Rap. Comm. Mass Spec.*, **5**(4), 175-187 (1991).
27. R. S. Mulliken, *J. Chem. Phys.*, **23**(10), 1841-1846 (1955).
28. H. Deutsch, *J. Appl. Phys.*, **89**(3), 1915-1921 (2001).
29. J. P. Desclaux, *Atom. Dat. Nucl. Dat.Tab.*, **12**(4), 311-406 (1973).
30. S. Kline and N. S. Jacobson, *Spreadsheet D-M Calculation of Atomic Cross Sections*, NASA Glenn Research Center (2012).
31. E. J. Opila, et al., *J. Am. Ceram. Soc.*, **82**(7), 1826-1834 (1999).
32. E. J. Opila and R.E. Hann, *J. Am. Ceram. Soc.*, **80**(1), 197-205 (1997).
33. K. Lee, N. Jacobson, and R. Miller, *MRS Bull.*, **19**(10), 35-38 (1994).
34. A. I. Zaitsev and B. M. Mogutnov, J. Mater. Chem., **5**(7), 1063-1073 (1995).
35. C. W. Bale, *Calphad*, **26**(2), 189-228 (2002).
36. P. Rocabois, C. Chatillon, and C. Bernard, *Rev. Intl. Hautes Temp. Refrac.*, **28**(2), 37-48 (1992).
37. R. C. Paule and J. L. Margrave, in *The Characterization of High-Temperature Vapors*, J.L. Margrave, Editor, John Wiley & Sons, New York (1967).
38. O. Fabrichnaya, et al., *Zeit. fur Metallk.*, **92**(9), 1083-1097 (2001).